

The H I Mass Function and Velocity Width Function of Void Galaxies in the Arecibo Legacy Fast ALFA Survey

Crystal M. Moorman,¹ Michael S. Vogele,¹ Fiona Hoyle,² Danny C. Pan,³
Martha P. Haynes,⁴ Riccardo Giovanelli⁴

1. Department of Physics, Drexel University, 3141 Chestnut Street, Philadelphia, PA 19104, USA

2. Pontificia Universidad Catolica de Ecuador, 12 de Octubre 1076 y Roca, Quito, Ecuador

3. Shanghai Astronomical Observatory, Shanghai, China, 200030

4. Center for Radiophysics and Space Research, Space Sciences Building, Cornell University Ithaca, NY 14853

Released 2014 Xxxxx XX

ABSTRACT

We measure the H I mass function (HIMF) and velocity width function (WF) across environments over a range of masses, $7.2 < \log(M_{\text{HI}}/M_{\odot}) < 10.8$, and profile widths, $1.3 \log(\text{km s}^{-1}) < \log(W) < 2.9 \log(\text{km s}^{-1})$, using a catalog of $\sim 7,300$ H I-selected galaxies from the ALFALFA Survey, located in the region of sky where ALFALFA and SDSS (Data Release 7) North overlap. We divide our galaxy sample into those that reside in large-scale voids (void galaxies) and those that live in denser regions (wall galaxies). We find the void HIMF to be well fit by a Schechter function with normalization $\Phi^* = (1.37 \pm 0.1) \times 10^{-2} h^3 \text{Mpc}^{-3}$, characteristic mass $\log(M_{\text{HI}}^*/M_{\odot}) + 2 \log h_{70} = 9.86 \pm 0.02$, and low-mass-end slope $\alpha = -1.29 \pm 0.02$. Similarly, for wall galaxies, we find best-fitting parameters $\Phi^* = (1.82 \pm 0.03) \times 10^{-2} h^3 \text{Mpc}^{-3}$, $\log(M_{\text{HI}}^*/M_{\odot}) + 2 \log h_{70} = 10.00 \pm 0.01$, and $\alpha = -1.35 \pm 0.01$. We conclude that void galaxies typically have slightly lower H I masses than their non-void counterparts, which is in agreement with the dark matter halo mass function shift in voids assuming a simple relationship between DM mass and H I mass. We also find that the low-mass slope of the void HIMF is similar to that of the wall HIMF suggesting that there is either no excess of low-mass galaxies in voids or there is an abundance of intermediate H I mass galaxies. We fit a modified Schechter function to the ALFALFA void WF and determine its best-fitting parameters to be $\Phi^* = 0.21 \pm 0.1 h^3 \text{Mpc}^{-3}$, $\log(W^*) = 2.13 \pm 0.3$, $\alpha = 0.52 \pm 0.5$ and high-width slope $\beta = 1.3 \pm 0.4$. For wall galaxies, the WF parameters are: $\Phi^* = 0.022 \pm 0.009 h^3 \text{Mpc}^{-3}$, $\log(W^*) = 2.62 \pm 0.5$, $\alpha = -0.64 \pm 0.2$ and $\beta = 3.58 \pm 1.5$. Because of large uncertainties on the void and wall width functions, we cannot conclude whether the WF is dependent on the environment.

Key words: cosmology: large-scale structure of the universe – cosmology: observations – galaxies: distances and redshifts – galaxies: luminosity function, mass function – methods: statistical

1 INTRODUCTION

The advent of large redshift surveys has allowed for a detailed mapping of the nearby Universe, revealing a variety of environments within which galaxies reside: rich clusters, groups, filaments, and the underdense regions filling the volume between. The starkly underdense regions filling most of our Universe, called “voids”, are relatively pristine environments for studying galaxy evolution and formation, because gas-stripping galaxy interactions are exceptionally rare. The study of galaxies living in these dynamically-distinct envi-

ronments is therefore crucial to understanding the processes that affect galaxy formation.

A variety of definitions of “voids” exists in the literature (El-Ad, Piran & da Costa 1997; El-Ad & Piran 1997, 2000; Plionis & Basilakos 2002; Sheth & van de Weygaert 2004; Hoyle & Vogele 2004; Rojas et al. 2004; Blanton et al. 2005a; Patiri et al. 2006; von Benda-Beckmann & Müller 2008; Melnyk et al. 2009; Karachentseva et al. 2010; Park et al. 2012; Sutter et al. 2012; Elyiv et al. 2013) ranging anywhere from locally isolated galaxies to extreme large-scale underdensities. We wish to focus on large-scale

structures and define voids as regions with density contrast $\delta < -0.8$ in optically-selected bright galaxies ($\sim L^*$) with a minimum radius of $10h^{-1}$ Mpc. That is, voids are not samples of “isolated” galaxies identified by visual inspection (e.g. Melnyk et al. 2009; Karachentseva et al. 2010). Large voids with density contrast $\delta < -0.8$ naturally arise via gravitational instability (Sheth & van de Weygaert 2004). These large-scale voids may be identified using a variety of void-finding algorithms including Kauffmann & Fairall (1991); El-Ad & Piran (1997); Aikio & Maehoenen (1998); Schaap & van de Weygaert (2000); Hoyle & Vogeley (2002); Neyrinck (2008); Aragon-Calvo et al. (2010). A comparison of different void-finding techniques may be found in Colberg et al. 2008. Studies reveal that large-scale voids occupy approximately 60 per cent of the volume of our Universe (Pan et al. 2012) and the galaxies within these voids form substructure that is evident in both simulations and observations (Mathis & White 2002; Benson et al. 2003; Gottlöber et al. 2003; van de Weygaert et al. 2010; Aragon-Calvo & Szalay 2013).

Simulations of the Λ CDM cosmological model predict an abundance of low-mass dark matter haloes (DMH) across all environments with a shift in the DMH mass function to lower masses in voids (Goldberg et al. 2005). If we assume a linear relationship between DMH mass, galaxy light and baryonic mass, then we expect to see an abundance of low-mass, low-luminosity galaxies in voids and denser regions as well. We know this assumption to be false, because star formation is suppressed at both high- and low-mass ends by e.g. AGN feedback and supernovae feedback, respectively. Given the phenomena affecting the low-mass ends, one might expect the low-mass slopes to vary across environment. For instance, ram pressure stripping removes cold gas from low-mass galaxies in clusters but this phenomenon would not be as prevalent in void galaxies. One might also expect the effects from supernovae to set in at a particular mass, yet it seems to affect both the void and wall galaxies similarly, regardless of the shift in characteristic mass between environment. To date, there is no evidence for a difference between the low-mass slopes in voids vs. denser regions, but we find this odd given the phenomena affecting the low-mass slopes. Critical points of comparison between the Λ CDM structure formation model and galaxy observations are found in the faint end of the galaxy luminosity function (LF) and the low-mass end of the neutral hydrogen mass function (HIMF). The global DMH mass function is predicted to follow a Schechter function (Press & Schechter 1974) with a very steep low-mass end slope ($\alpha \simeq -1.8$; Mathis & White (2002)), but measurements of the observed faint and low-mass end slopes of the global galaxy LF (e.g. Blanton et al. (2005b)) and HIMF (e.g. Martin et al. (2010)) are significantly shallower ($\alpha \simeq -1.3$). While Blanton et al. (2005b) note that selection effects of low-surface brightness galaxies could cause the slope to flatten, their estimate of the corrected slope is still too shallow ($\alpha \simeq -1.5$) to match DMH predictions.

Studies focusing on galaxies in large-scale voids indicate that void galaxies are generally bluer, fainter, later-type, and have higher star formation rates (SFRs) per stellar mass than their counterparts in denser regions (Rojas et al. 2004, 2005; Hoyle et al. 2005; Blanton et al. 2005a; Croton et al. 2005; Park et al. 2007; Croton & Farrar 2008; Cen 2011;

Kreckel, Joung & Cen 2011; Hoyle, Vogeley & Pan 2012; Geha et al. 2012). Optical observations also reveal a discrepancy between the number of low-luminosity/low-mass (dwarf) galaxies and the predicted number of low-mass haloes (e.g. Karachentsev et al. 2004). This discrepancy is part of the void problem mentioned in Peebles (2001) which states that all types of galaxies appear to respect the voids, whereas Λ CDM predicts that voids should contain an abundance of low mass objects. Λ CDM simulations (Warren et al. 2006; Hoefft et al. 2006) predict that voids have a density of low-mass haloes that is 1/10 that of the cosmic mean. This is consistent with bright galaxies in large scale voids (Hoyle & Vogeley 2004; Conroy et al. 2005; Hoefft et al. 2006; Tinker et al. 2008); however, optical observations do not reveal a plethora of faint galaxies in voids (e.g. Karachentsev et al. (2004); in the Local Void). Among the attempts to identify an abundance of dwarf galaxies in voids are Grogin & Geller (1999); Blanton et al. (2003a); Hoyle et al. (2005); Croton et al. (2005) and Hoyle, Vogeley & Pan (2012) who investigate the environmental dependence of the LF of optically-selected galaxies. These results vary depending on the definition of environment used in the work, and none identifies an excess of dwarf galaxies in extreme voids. Kuposov et al. (2009) propose that the lack of dwarf galaxies in voids found in optically-selected samples could be due to strong star formation suppression of void galaxies, before and after reionization, as well as observational selection effects. If these effects are responsible, we would expect a population of low-mass, optically-dark, yet H I-rich galaxies to exist. Such a population should be detectable by their gas.

The results of Basilakos et al. (2007) indicate that low H I-mass galaxies seem to avoid underdense regions. To date, with only a handful of exceptions (e.g. Giovanelli et al. 2013), evidence of a population of gas-rich, optically dark galaxies large enough to reconcile dwarf galaxy counts with Λ CDM models does not exist (Haynes 2008). The first generation of blind H I surveys were typically shallow and unable to detect H I clouds over a large range of masses. Small number statistics and uncertainties in distances of nearby galaxies (Masters, Haynes & Giovanelli 2004) made determining large scale environmental effects on galactic H I content difficult. Haynes, Giovanelli & Chincarini (1984) show that environment has an impact on the H I content of galaxies, where galaxies in clusters tend to be more H I deficient than “field” galaxies. Using the Arecibo Dual Beam Survey (Rosenberg & Schneider 2000), Rosenberg & Schneider (2002) corroborate this work hinting at the influence of large scale structure on the HIMF. These authors show that, for galaxies in the Virgo Cluster, the low-mass-end slope of the HIMF becomes shallower.

With the onset of deeper, large area blind-H I surveys, we are able to better constrain the environmental impact on a galaxy’s H I content. Headway has been made on determining the environmental dependence of the HIMF of H I clouds from second generation surveys by Zwaan et al. (2005) using the H I Parkes All Sky Survey (HIPASS; Meyer et al. 2004) and by Springob, Haynes & Giovanelli (2005), Stierwalt et al. (2009), and Martin (2011) using various data releases from the ALFALFA Survey (Giovanelli et al. 2005a,b). We find in the literature that the low-mass end slope of the HIMF may become steeper or

shallower with density depending on sample selection and the definition of environment. See, for example, Zwaan et al. (2005), Springob, Haynes & Giovanelli (2005), Toribio et al. (2011), and Martin (2011) who use either H I- or optically-selected samples to define the environment of H I-selected galaxies on scales ranging from locally isolated galaxies to low density environments on scales of ~ 10 Mpc. We discuss the conflicting HIMF results in more detail below in Section 4.1.

Another point of comparison between Λ CDM simulations and observations is through estimating corrections to the velocity width function (WF) to obtain a circular velocity function, although this comparison is less direct. Cold dark matter models predict the circular velocity functions of haloes to follow a power law with a steep slope of $\alpha \sim -3$ (Klypin et al. 1999; Zavala et al. 2009). Observations do not confirm this prediction. In fact, the observed velocity functions closely resemble Schechter functions with much shallower low-velocity slopes (e.g. Sheth et al. 2003; Zwaan, Meyer & Staveley-Smith 2010; Papastergis et al. 2011). The observed velocity function of galaxies may be obtained indirectly through optical photometry or spectra using of the Tully-Fisher relation (Desai et al. 2004; Abramson et al. 2013) or through direct observations of the velocity width using H I surveys (Zwaan, Meyer & Staveley-Smith (2010) with HIPASS; Papastergis et al. (2011) with ALFALFA).

A comparison of previous work on both optically-selected void galaxies and H I-selected galaxies reveal similar characteristics between these two samples. Toribio & Solanes (2009) investigate properties of “isolated” H I-selected galaxies from ALFALFA and find that these remote objects tend to be blue, late-type, star-forming galaxies. Huang et al. (2012) compare properties of H I- and optically-selected samples found within the volume covered by both SDSS DR7 and ALFALFA and find that for a given stellar mass, H I-selected galaxies generally have higher star formation rates and specific star formation rates, yet lower star formation efficiencies. Rojas et al. (2004); Hoyle et al. (2005); Hoyle, Vogeley & Pan (2012) find that optically-selected void galaxies are generally bluer, fainter, late-type, and have higher specific star formation rates than galaxies in denser regions. Given the similarities in the characteristics of galaxies detected by blind H I surveys and void galaxies found using optically-selected data, we would expect that H I surveys yield a higher fraction of void galaxy detections than that of galaxies found using optical surveys. As discussed in more detail below, we find that 33 per cent of ALFALFA detections reside in large scale voids, while in the same volume (out to $z \sim 0.5$) 26 per cent of magnitude-limited SDSS detections are classified as void galaxies.

In this paper, we study the HIMF and WF of ALFALFA galaxies that lie in deep large-scale voids. In Section 2 we discuss our void catalog and H I-selected sample. In Section 3 we present our methods and results for the HIMF and WF of void galaxies. We compare our results to previous work in Section 4 and summarize our results in Section 5. Unless otherwise specified, we adopt the distances, D_i ; H I masses, M_{HI} ; velocity widths, W_{50} ; and integrated H I fluxes, S_{int} reported in the $\alpha.40$ catalog (Haynes et al. 2011), as well as the ALFALFA adopted Hubble constant $h = H_0/100$ km

$\text{s}^{-1}\text{Mpc}^{-1} = 0.7$. Where comoving coordinates are determined, we assume $\Omega_m = 0.26$ and $\Omega_\Lambda = 0.74$.

2 DATA

2.1 Finding A Void Galaxy Sample Using SDSS DR7

The Sloan Digital Sky Survey Data Release 7 (SDSS DR7) (Abazajian et al. 2009) is a wide-field multi-band imaging and spectroscopic survey that uses drift scanning to map $8,032 \text{ deg}^2$ of the northern sky. SDSS utilizes the 2.5m telescope located at Apache Point Observatory in New Mexico, allowing it to cover $\sim 10^4 \text{ deg}^2$ of the northern hemisphere in the five band SDSS system- $u, g, r, i,$ and z (Fukugita et al. 1996; Gunn et al. 1998). Galaxies with Petrosian r -band magnitude $r < 17.77$ are selected for spectroscopic follow up (Lupton et al. 2001; Strauss et al. 2002). Spectra obtained through the SDSS are taken using two double fiber-fed spectrographs and fiber plug plates covering a portion of the sky 1.49° in radius with a minimum fiber separation of 55 arcseconds (Blanton et al. 2003b).

The Korea Institute for Advanced Study Value-Added Galaxy Catalog (KIAS-VAGC) of Choi, Han & Kim (2010) is based on the SDSS DR7. This consists of 583,946 galaxies with $10 < r < 17.6$ from the NYU-VAGC Large Scale Structure Sample (brvoid0) (Blanton et al. 2005c), 114,303 galaxies with $17.6 < r < 17.77$ from NYU-VAGC (full0), and 10,497 galaxies from either UZC, PSCz, RC3, or 2dF which were excluded by SDSS. We omit 929 objects, mostly de-blended outlying parts of large galaxies, for a total of 707,817 galaxies.

To create a void catalog, Pan et al. (2012) employ the void finding algorithm of Hoyle & Vogeley (2002), called VoidFinder – based on the El-Ad & Piran (1997) approach – on a volume limited sample of the KIAS-VAGC. The volume-limited sample we use consists of 120,606 galaxies within $z = 0.107$ corresponding to an absolute magnitude limit of $M_r < -20.09$. VoidFinder uses a nearest neighbors algorithm to identify volume-limited galaxies in low density regions. If a galaxy’s third nearest neighbor is at least $6.3h^{-1}$ Mpc away it is considered a potential void galaxy and is removed from the sample. VoidFinder then grows spheres in the empty spaces until the spheres are bounded by four remaining galaxies. If the sphere has a radius larger than $10h^{-1}$ Mpc it is considered a void, otherwise it is discarded. Each void is comprised of multiple spheres and we define the centre of each void to be the centre of the sphere with the maximal radius. The VoidFinder parameters were chosen to select void regions with density contrast $\delta < -0.8$. For a more detailed description of how VoidFinder works, see Hoyle & Vogeley (2002) and Pan et al. (2012).

Pan et al. (2012) identify 1,054 voids with radii greater than $10h^{-1}$ Mpc occupying approximately 60 per cent of the volume covered by the SDSS DR7 out to $z=0.107$. These voids have less than 10 per cent of the average density out to the walls. They are ellipsoidal in shape with a preference for being prolate. The median effective void radius is $15h^{-1}$ Mpc with over half of the volume consisting of voids with effective radius greater than $17.8h^{-1}$ Mpc. Figure 1 shows a $10h^{-1}$ Mpc thick redshift slice of the volume-limited sample used

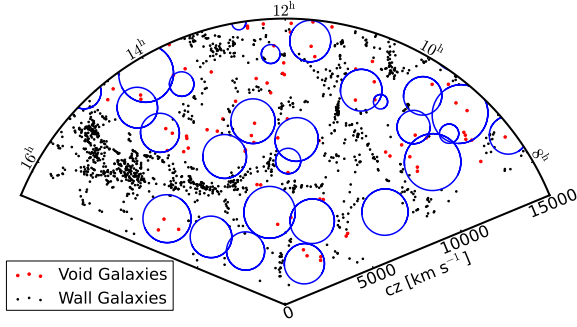


Figure 1. $10h^{-1}$ Mpc slab of SDSS DR7 volume-limited sample. Void galaxies are displayed as red points, and wall galaxies are displayed as black points. The circles depict the intersection of only the maximal sphere of a void with the centre of the slice. Note that voids tend to be ellipsoidal rather than spherical, thus void galaxies may appear outside of the maximal sphere drawn.

to identify large-scale voids, centred at R.A.= 12^h , Dec= 10° . Wall galaxies in the volume-limited sample are shown as black points and void galaxies are shown as red points. The circles depict the intersection of the maximal spheres of each void with the centre of the slice.

To account for the effects of the local peculiar velocity field, we apply the FlowModel of Masters (2005) to the KIAS-VAGC galaxies. We then create a volume-limited sample with absolute magnitude limit $M_r < -20.09$. We apply the VoidFinder algorithm to this volume-limited sample. See Figure 2 for the resulting void locations after applying the FlowModel to the KIAS sample compared to those of Pan et al. (2012). This figure depicts the same region of sky shown in Figure 1 with the intersection of the centre of the slab with the modified void catalog alongside the intersection of the slab with the Pan et al. (2012) void catalog. Comparing galaxy locations to the void catalog found using the FlowModel does not result in a significant difference in void and wall galaxy samples (see Figure 3). Because we do not notice a significant difference between the void catalog of Pan et al. (2012) and our void catalog, we use the void catalog of Pan et al. (2012) for consistency.

2.2 The ALFALFA Sample

The Arecibo Legacy Fast ALFA (ALFALFA) Survey is a large-area, blind extragalactic H I survey that will detect $>30,000$ galaxies out to $cz \sim 18000 \text{ km s}^{-1}$ with a median redshift of $\sim 8,000 \text{ km s}^{-1}$, over 7000 deg^2 of sky upon completion. ALFALFA has a 5σ detection limit of $0.72 \text{ Jy km s}^{-1}$ for a source with a profile width of 200 km s^{-1} (Giovanelli et al. 2005a) and allows for the detection of galaxies with H I masses down to $M_{\text{HI}} = 10^8 M_\odot$ out to 40 Mpc. The most recent release of the ALFALFA Survey (Giovanelli et al. 2005a,b), the $\alpha.40$ catalog of Haynes et al. (2011), covers $\sim 2800 \text{ deg}^2$, approximately 40 per cent of the final survey area. This catalog, which consists of 15,041 H I detections and contains previously released catalogs (Giovanelli et al. 2007; Saintonge et al. 2008; Kent et al. 2008; Stierwalt et al. 2009; Martin et al. 2009), covers two regions in the northern Galactic Hemisphere, referred to as

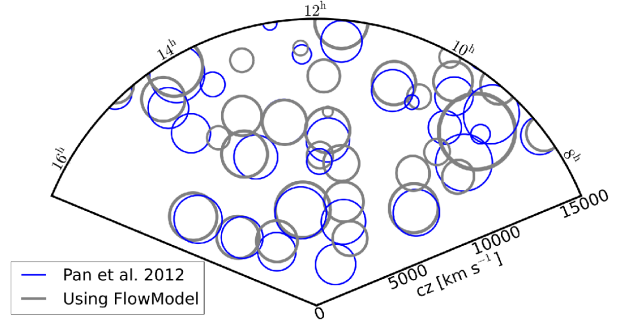


Figure 2. We process the KIAS data set through the FlowModel of Masters et al. (2005) and obtain a new volume-limited sample to run through VoidFinder. This figure depicts the intersection of the centre of a $10h^{-1}$ Mpc slab centred at R.A.= 12^h , Dec= 10° with the resulting maximal spheres of this new set of voids (gray circles). For comparison, we also show the intersection of the slab with the maximal void spheres of the Pan et al. 2012 void catalog (blue circles) found using an SDSS DR7 volume-limited sample.

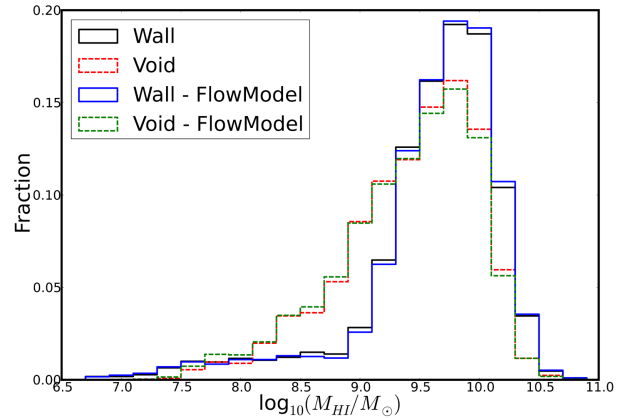


Figure 3. H I mass distribution of void (red dashed line) and wall (black solid line) galaxies as determined by the Pan et al. (2012) void catalog and the H I mass distribution of void (green dashed line) and wall (blue solid line) galaxies as determined by the modified void catalog obtained using the FlowModel of Masters et al. (2005).

the Spring Sky, ($07^h 30^m < \text{R.A.} < 16^h 30^m$, $04^\circ < \text{Dec} < 16^\circ$ and $24^\circ < \text{Dec} < 28^\circ$), and two in the southern Galactic Hemisphere, referred to as the Fall Sky, ($22^h < \text{R.A.} < 03^h$, $14^\circ < \text{Dec} < 16^\circ$ and $24^\circ < \text{Dec} < 32^\circ$). Haynes et al. (2011) categorize the confidently detected H I sources of the $\alpha.40$ catalog into one of three categories: Code 1 objects are reliable detections with high signal-to-noise ratio ($S/N > 6.5$), Code 2 objects have lower S/N , but coincide with optical counterparts with known redshift similar to that of the H I detection, and Code 9 objects which correspond to high velocity clouds (HVCs).

Our interest lies in identifying reliable H I detections in voids. To identify $R > 10h^{-1}$ Mpc voids, VoidFinder requires wide angular coverage in spectroscopy, which for SDSS DR7, is only possible in North. This region of sky corresponds to

the ALFALFA Spring Sky, thus we reduce our sample to objects included only in the Spring Sky. We further limit ourselves to Code 1 detections which lie within the redshift range $cz \leq 15000 \text{ km s}^{-1}$; beyond this redshift range, the FAA radar at the San Juan Airport interferes with ALFALFA's detection ability over a range of frequencies corresponding to a shell of thickness ~ 10 Mpc. Our final sample contains 8,118 H I sources over an area of 2,077 deg^2 corresponding to ~ 30 per cent of the final projected survey area.

To ensure that we are using an unbiased H I-selected sample, we use the aforementioned subset of the full $\alpha.40$ data set to determine the HIMF and WF of void galaxies. However, certain tasks we would like to accomplish (namely those in Sections 3.2.1) require that we cross-match the H I-detections with optical galaxies. Haynes et al. (2011) supply a cross-reference of 12,468 ALFALFA H I sources with the most probable optical counterpart from the SDSS DR7 where the two survey footprints overlap. Of the original 15,041 H I detections in the $\alpha.40$ catalog, 201 have no assigned optical counterpart, 2312 lie outside the SDSS DR7 footprint, and 60 appear within the SDSS DR7 imaging survey but the galaxies' images are contaminated by bright foreground stars or other artefacts. From the cross-referenced catalog, we obtain photometric object IDs and query the SDSS DR7 database to obtain information regarding the apparent magnitude in each Sloan filter for every object in order to identify the objects' colour and absolute r -band magnitude, M_r . Because we are comparing optically-selected galaxy LFs to H I-selected galaxy LFs, we wish to remain consistent in how we determine absolute magnitudes; therefore, we K -correct the magnitudes and band-shift each H I source's M_r to $z = 0.1$ using K -correct Version 4.4 (Blanton & Roweis 2007) as done in the KIAS-VAGC.

3 METHODS

3.1 Creating a Void H I-Selected Sample

We categorize the H I sources within our sample into void and wall galaxy samples by comparing the coordinates of each galaxy to the void catalog of Pan et al. (2012). The void locations are found using comoving coordinates; to ensure we are consistent in finding the locations of H I clouds with respect to the voids, we use the redshift of each detection to obtain its comoving coordinates in h^{-1} Mpc. From our H I-detected sample, we identify 2,777 (33%) void galaxies and 4,857 (60%) wall galaxies. The remaining 384 (6%) ALFALFA detections lie near the edges of the SDSS DR7 mask, so we cannot determine whether the galaxies live in a bonafide void. If we imagine there is a spherical void with radius $11h^{-1}$ Mpc lying only half in the survey, VoidFinder would be unable to fit a $10h^{-1}$ Mpc sphere within the survey in this region, so any galaxies in the spherical void would not be identified as void galaxies. Galaxies living all along the boundaries of the SDSS mask could be affected by such misclassifications; therefore, we remove these galaxies from our analysis so as not to contaminate our wall sample. Even with the removal of these edge galaxies, we are still sampling a cosmologically significant volume.

We encourage the reader to keep in mind that when

we refer to “void” and “wall” galaxies in this paper, the names are not synonymous with “void” and “wall” galaxies referred to in other papers that have utilized VoidFinder as a means of identifying large-scale voids. The classification of voids and walls is the same as seen elsewhere, but the samples of galaxies within those environments differs because of the differences in H I-selected vs. optically-selected samples. In this paper, we are identifying the void and wall galaxies of a blind H I survey. The galaxy sample used here and those used elsewhere are very different; for example, blind H I detections residing in walls rarely populate the densest regions of the walls where we find a proliferation of galaxies in the optical. Optically-selected wall samples typically consist of galaxies from the red sequence. By using an H I-selected sample, we lose a significant portion of the red sequence, and thus reduce the raw count of the wall population. This reduction of the wall population, results in an increased void fraction for H I-selected samples. For comparison, within the same volume ($z \leq 0.5$), ~ 26 per cent of SDSS DR7 galaxies reside in voids. Note that one must be careful in computing the void fraction of a sample. Calculating the numerator is straight forward and is defined as simply the number of objects residing in voids; while the denominator must include only the galaxies accessible to VoidFinder. Excluded from the denominator are galaxies beyond a specified redshift (here, $z \leq 0.5$) and galaxies lying very near to the survey boundaries as discussed above.

We present the distribution of H I masses of void and wall galaxies of our ALFALFA sample in Figure 4. Here, we notice void galaxies tend to have lower H I masses than wall galaxies. Figure 5 shows our ALFALFA sample in a $10h^{-1}$ Mpc thick redshift slice centred at R.A.= 12^h , Dec= 10° . This is the same slice depicted in Figure 1 where, again, wall galaxies are shown as black points, void galaxies are shown as red points, and circles depict the intersection of the maximal spheres of each void with the centre of the slice. The nearby voids appear highly populated by ALFALFA galaxies. The reader should keep in mind that Figure 5 plots an H I flux limited sample, whereas Figure 1 depicts an optical volume-limited sample; thus the majority of galaxies corresponding to these H I detections found in voids are fainter than our volume-limited cut of $M_r < -20.09$.

In addition to these physical boundary cuts, the method that we apply in this paper, the two dimensional stepwise maximum likelihood (2DSWML) method, requires that our sample be complete; therefore, we eliminate all galaxies that fall below the 50 per cent completeness threshold in the flux-width plane reported in Section 6 of Haynes et al. (2011). Figure 6 depicts the distribution of H I detections described in Section 2.2 with this completeness threshold in the flux-width plane. This cut eliminates 152 void galaxies and 240 wall galaxies. We provide a brief explanation of the completeness cuts here. Haynes et al. (2011) begin by separating the ALFALFA detections into H I line-width bins, then within each width bin the galaxies are binned again by integrated H I flux. A flux-limited sample from a uniform distribution of galaxies will produce a number count that approximately follows a power law with slope $-3/2$. The authors determine the onset of incompleteness when the binned integrated flux data deviate from this form. In Figure 7, we present the distribution of the final sample used in our analysis in the mass-width plane.

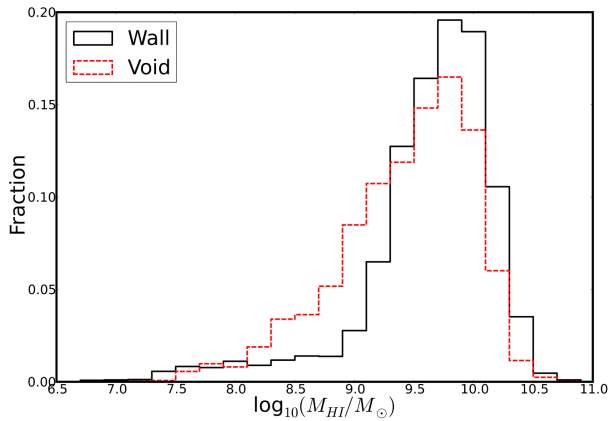


Figure 4. H I Mass distribution of void (red dashed line) and wall (black solid line) galaxies. The relatively small number of nearby structures makes it imperative that we use an inhomogeneity-independent method to estimate the H I mass function of this dataset. H I detections living in voids typically have lower H I masses than those in denser regions.

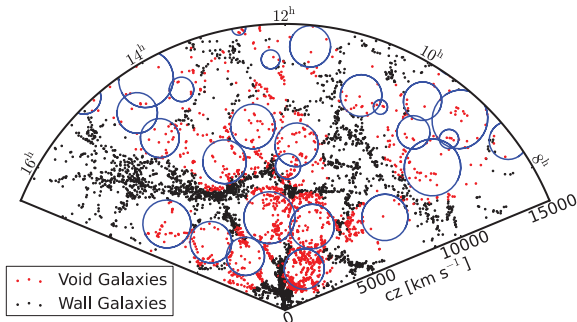


Figure 5. $10h^{-1}$ Mpc slab of ALFALFA detections in the Spring Sky. Void galaxies are displayed as red points, wall galaxies are displayed as black points, and galaxies too close to the SDSS mask edge were not plotted. The circles depict the intersection of the maximal sphere of a void with the centre of the slice. The voids appear highly populated, but the galaxies corresponding to the H I detections are fainter than the $M_r < -20.09$ galaxies used in our volume-limited catalog. Refer to Figure 1 for the volume-limited sample used to produce the voids this slice.

We make cuts to the ALFALFA-SDSS cross-referenced catalog identical to the ones mentioned in Section 2.2. The resulting subsample is 305 H I detections fewer than the full sample mentioned above. We lose 54 H I detections from the void sample, 132 detections from the wall sample, and 119 from the edges where the survey region is inaccessible to VoidFinder. We further limit this sample to objects lying only in the ALFALFA Spring Sky. These reductions leave us with 7404 H I detections. 2571 of these live in voids, while 4485 reside in denser regions. The remainder of the galaxies lie along the edge of the SDSS DR7 survey mask in regions inaccessible to VoidFinder.

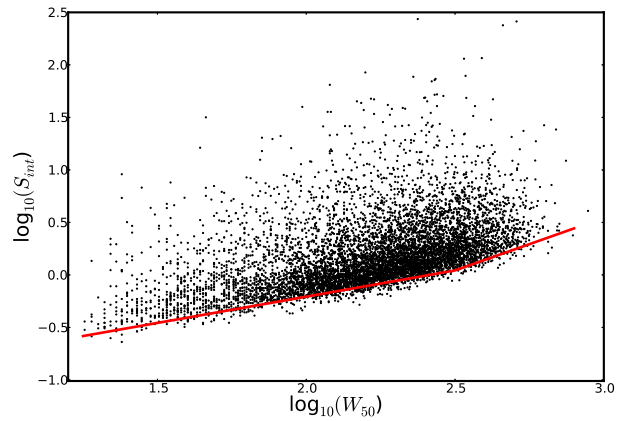


Figure 6. Distribution of H I detections used in this paper shown in integrated flux vs. velocity width space. The red line indicates our adopted completeness limit which is the 50 per cent completeness threshold reported in Haynes et al. 2011.

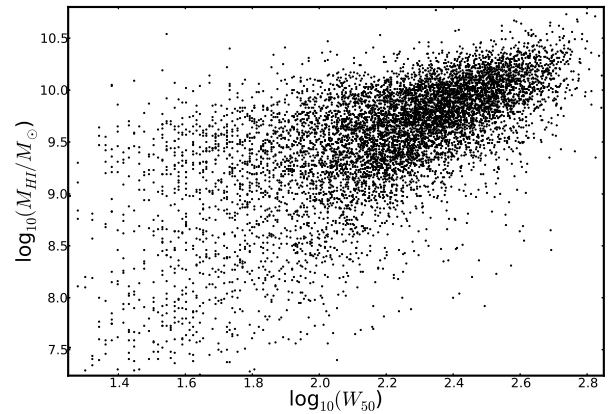


Figure 7. Distribution of our final sample in H I mass vs. velocity width space after all cuts have been made. The completeness limit of the sample in this space is dependent on the distance to each object and cannot be depicted using a single line.

3.2 The 2DSWML Method

Because the ALFALFA survey's detection limit is dependent on both H I mass and velocity width (Giovanelli et al. 2005b), we estimate the H I mass function (HIMF) and the velocity width function (WF) of our ALFALFA void and wall samples using an extension of the stepwise maximum likelihood method of Efstathiou, Ellis & Peterson (1988) called the bivariate or two-dimensional stepwise maximum likelihood (2DSWML) method, introduced by Loveday (2000). We provide a brief overview of the 2DSWML method here. For more details of the direct application of this method to the $\alpha.40$ sample, see Martin et al. (2010, Appendix B).

We obtain our estimates of the HIMF and WF by first splitting the bivariate distribution function $\phi(M_{\text{HI}}, W_{50})$ into bins and define ϕ_{jk} as the maximum likelihood parameter of the distribution in logarithmic mass bin j and

logarithmic velocity width bin k . We attain the maximum likelihood solution via iteration of the following equation obtained by Efstathiou, Ellis & Peterson (1988):

$$\phi_{jk} = \frac{n_{jk}}{\sum_i \frac{H_{ijk}}{\sum_m \sum_n H_{imn} \phi_{mn}}}. \quad (1)$$

Here, n_{jk} is the number of galaxies within each bin in the mass-width plane and H_{ijk} is a function that ensures the summation only goes over the area of bins accessible to galaxy i , where

$$H_{ijk} = \frac{1}{\delta M_{\text{HI}} \delta W_{50}} \int_{W_k^-}^{W_k^+} \int_{M_j^-}^{M_j^+} C_i(M_{\text{HI}}, W_{50}) dM_{\text{HI}} dW_{50}. \quad (2)$$

Here $C_i(M_{\text{HI}}, W_{50})$ is an approximation of the completeness function described in Haynes et al. 2011 in the mass-width plane for galaxies at distance D_i . That is, if an object's integrated flux falls below the completeness limit, $C=0$, otherwise $C=1$. M_j^- and M_j^+ are the lower and upper limits on logarithmic mass bin j , and similarly, W_k^- and W_k^+ are the lower and upper limits on logarithmic width bin k .

After obtaining the maximum likelihood bivariate distribution parameters, ϕ_{jk} , we marginalize over velocity width to measure the HIMF. Because the normalization is lost, we match the normalization of the void and wall galaxy HIMFs to the number density of void and wall galaxies within their respective volumes. We compare our measurements of the void and wall galaxy HIMFs over the mass range $7.2 < \log(M_{\text{HI}}/M_{\odot}) < 10.8$ with a Schechter function (Schechter 1976) of the form

$$\Phi(M_{\text{HI}}) = \frac{dN}{d \log M_{\text{HI}}} = \ln 10 \Phi^* \left(\frac{M_{\text{HI}}}{M^*} \right)^{(\alpha+1)} \times \exp \left(-\frac{M_{\text{HI}}}{M^*} \right). \quad (3)$$

We estimate the normalization factor Φ^* , the characteristic gas mass M^* , and the low-mass-end slope α using a least squares estimator.

Here we present the global HIMF of the full $\alpha.40$ data set. It is well fit by a Schechter function with estimated parameters ($\Phi^* = (6.3 \pm 0.3) \times 10^{-3} \text{Mpc}^{-3}$, $\log(M^*/M_{\odot}) + 2 \log h_{70} = 9.96 \pm 0.02$, $\alpha = -1.33 \pm 0.02$) similar to those of Martin et al. (2010): $\Phi^* = (4.8 \pm 0.3) \times 10^{-3} \text{Mpc}^{-3}$, $\log(M^*/M_{\odot}) + 2 \log h_{70} = 9.96 \pm 0.02$, $\alpha = -1.33 \pm 0.02$. Limiting the data set to H I detections located in the Spring Sky, we do not see a significant difference in the best-fitting parameters of the HIMF ($\Phi^* = (5.34 \pm 0.4) \times 10^{-3} \text{Mpc}^{-3}$, $\log(M^*/M_{\odot}) + 2 \log h_{70} = 9.97 \pm 0.02$, $\alpha = -1.35 \pm 0.04$).

Dividing the Spring Sky into void and wall galaxies produce the following results: In Figure 8 we present the HIMF of both void and wall galaxy samples. For the void sample, we estimate the best-fitting Schechter parameters to be $\Phi^* = (1.37 \pm 0.1) \times 10^{-2} \text{Mpc}^{-3}$, $\log(M^*/M_{\odot}) + 2 \log h_{70} = 9.86 \pm 0.02$, $\alpha = -1.29 \pm 0.02$. For the wall galaxy sample, we estimate $\Phi^* = (1.82 \pm 0.03) \times 10^{-2} \text{Mpc}^{-3}$, $\log(M^*/M_{\odot}) + 2 \log h_{70} = 10.00 \pm 0.01$, $\alpha = -1.35 \pm 0.01$. See Section 3.3 for an explanation of uncertainties. The curves in Figure 8 show the Schechter functions associated with these best-fitting parameters.

We see that $\log(M^*)$ shifts towards lower H I masses in voids by $\log(M^*) = 0.14$. This characteristic mass is shifted

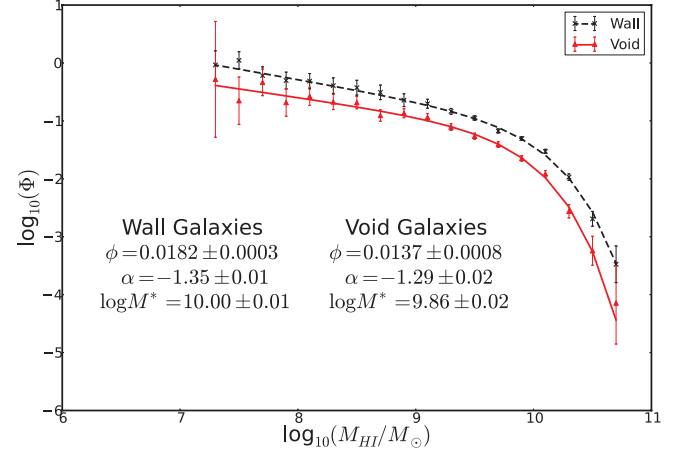


Figure 8. The HIMF of void (red) and wall (black) galaxies. The best-fitting Schechter functions for each sample are shown as solid (void) and dashed (wall) lines. We notice a shift towards lower masses as well as a small decrease in the low-mass slope for void galaxies.

by a factor of 1.4 and the direction of this shift is consistent with the shift in the DMH mass function of extended Press-Schechter theory (Goldberg et al. 2005). This direction of the shift is also in agreement with the shift in the optical LF. We cannot quantitatively compare our HIMF shift with the shift found in the optically-selected LF from voids to walls because of a difference in sample selection, but for completeness, Hoyle et al. (2005) find a shift in LF of the r -band magnitude towards lower magnitudes of $M_r^* \sim 1$ for void galaxies (a factor of 2.5). We also see only a slight dependence of the low-mass slope, α , on environment, with the slope steepening with increasing density. We compare our results to previous work more completely later in Section 4, but for now we will briefly compare our HIMF results to the HIMF of the Leo Group (Stierwalt et al. 2009), who estimate a low-mass slope of $\alpha = -1.41 \pm 0.04$ using ALFALFA. Given our findings, we conclude that the low-mass slope of the HIMF for ALFALFA galaxies in the Spring Sky is shallow for voids. The slope may increase with density to arrive at the steep Leo I Group slope, but the slope does not necessarily increase monotonically with density. Depending on how densely packed a particular galactic group or cluster is, the low-mass slope of the HIMF may vary drastically, ranging anywhere from the steep slope of the Leo Group (Stierwalt et al. 2009) to the very flat slopes found in loose groups (Pisano et al. 2011) and clusters (Verheijen et al. 2001; Rosenberg & Schneider 2002; Martin 2011) which, when combined, may give an intermediate low-mass slope similar to that of our wall galaxy sample.

3.2.1 WF

To determine the velocity width function, we obtain our results from the bivariate distribution function of the 2DSWML method and marginalize over H I mass. As with the HIMFs, we must match the normalization of the void and wall WFs to their respective densities. To remain consistent with previously reported ALFALFA WF results

(Papastergis et al. 2011 obtain observational results and translate theoretical results to the observed quantity rather than estimate corrections for the observations), we have corrected the velocity widths for Doppler broadening and make no other corrections, e.g. galaxy inclination. We compare the void and wall galaxy width functions over the width range $1.3 \log(\text{km s}^{-1}) < \log(W_{50}) < 2.9 \log(\text{km s}^{-1})$, where W_{50} is the velocity width measured at 50 per cent of the peaks of the H I-line profile. The high velocity width end falls off too quickly to be well fit by a Schechter function, so we fit the WFs to a modified Schechter function of the form

$$\Phi(W_{50}) = \frac{dN}{d \log W_{50}} = \ln 10 \Phi^* \left(\frac{W_{50}}{W^*} \right)^\alpha \exp \left(- \frac{W_{50}}{W^*} \right)^\beta \quad (4)$$

and estimate the normalization factor Φ^* , the characteristic velocity width $\log W^*$, and the low and high velocity width slopes α and β using a least squares estimator.

Here we present the global WF of the full $\alpha.40$ sample. It is well fit by a modified Schechter function where our 2DSWML-estimated parameters ($\Phi^* = (2.1 \pm 0.2) \times 10^{-2} \text{Mpc}^{-3}$, $\log(W^*) = 2.56 \pm 0.03$, $\alpha = -0.73 \pm 0.02$, $\beta = 2.6 \pm 0.2$) match closely those of Papastergis et al. (2011): $\Phi^* = (1.1 \pm 0.2) \times 10^{-2} \text{Mpc}^{-3}$, $\log(W^*) = 2.58 \pm 0.03$, $\alpha = -0.68 \pm 0.11$, $\beta = 2.7 \pm 0.3$. Limiting the data set to H I detections located in the Spring Sky, the WF remains well fit by a modified Schechter function although the parameters change somewhat: $\Phi^* = (1.3 \pm 0.3) \times 10^{-2} \text{Mpc}^{-3}$, $\log(W^*) = 2.61 \pm 0.03$, $\alpha = -0.91 \pm 0.02$, $\beta = 3.44 \pm 0.2$. When we divide the Spring Sky sample into void and wall galaxies, our results of the 2DSWML method change drastically. In Figure 9 we present the WF of both void and wall galaxy samples. We see these functions are not as well fit by the modified Schechter function as the global $\alpha.40$ WF (see Figure 4 in Papastergis et al. 2011). For the void sample, we estimate the best-fitting modified Schechter parameters to be $\Phi^* = 0.21 \pm 0.1 \text{Mpc}^{-3}$, $\log(W^*) = 2.13 \pm 0.3$, $\alpha = 0.52 \pm 0.5$, $\beta = 1.3 \pm 0.4$. For the wall galaxy sample, we estimate $\Phi^* = 0.022 \pm 0.009 \text{Mpc}^{-3}$, $\log(W^*) = 2.62 \pm 0.5$, $\alpha = -0.64 \pm 0.2$, $\beta = 3.58 \pm 1.5$. We note here that two bins in both the void and wall WFs appear to be extreme outliers (void: $\log(W_{50}) = 1.8, 2.6$; wall: $\log(W_{50}) = 1.5, 2.0$), however these bin heights are not caused by low-number statistics. The curves in Figure 9 show the modified Schechter functions associated with these best-fitting parameters.

We see that W^* shifts towards lower velocity widths in voids compared to walls; however, due to large uncertainties, we are unable to make any conclusive statements about the other parameters. It is our goal to ascertain whether there are any differences in the WF of void galaxies and wall galaxies. Looking at the poorly-fit Schechter functions gives us no real insight, so we compute a Kolmogorov–Smirnov test to compare the wall and void WF distributions. Including all points in the distributions (note the outlying points), we obtain a p-value of 0.05 from the K-S test. That is, 95 per cent of the time we would correctly reject the hypothesis that the void and wall WFs are drawn from the same distribution. We have no reason to exclude the extreme outliers, but excluding the extreme outliers, yields a p-value of 0.07. See Figure 10 for a comparison of the CDFs of the two distributions with and without the outliers.

As mentioned above, galaxies in voids tend to be blue,

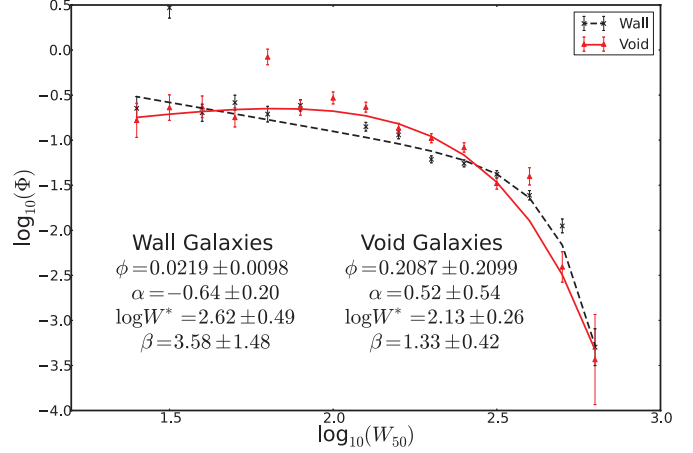


Figure 9. The WF of void (red) and wall (black) galaxies. The best-fitting modified Schechter functions for each sample are shown as solid (void) and dashed (wall) lines. Neither the void nor wall WF is well fit by a modified Schechter function.

late-type galaxies whereas red, dead, elliptical galaxies are primarily found in denser regions of the Universe. Therefore, we investigate the effects of colour to shed some light on possible explanations as to why/if the WF differs between void and wall galaxies. For this sample, we use the ALFALFA-SDSS cross-reference catalog provided by Haynes et al. (2011). This results in a few less galaxies than the sample we have been working with because we are dependent on the SDSS photometric pipeline for matches, and in some cases, the galaxy images may be contaminated by a foreground star or other artefact.

We split our H I cloud sample into groups based on colour where we define galaxies with a colour $u - r < -0.09M_r + 0.46$ as blue and galaxies with colour $u - r \geq -0.09M_r + 0.46$ as red. Here, M_r is the r -band magnitude of the object’s optical counterpart given by the SDSS DR7. See Figure 11 for the location of this definition of colour as shown on a colour-magnitude diagram; this cut divides the sample into a “red sequence” and a “blue cloud”. Our resulting subsamples contain $\sim 6,000$ blue galaxies and $\sim 1,400$ red galaxies. Figure 12 depicts the resulting WFs of the blue and red subsamples along with the best-fitting modified Schechter functions. We see that the low-width slope of the red galaxy WF is substantially flatter than that of the blue galaxies. Because a blind-H I survey is more likely to identify a blue, late-type galaxy (e.g. Huang et al. 2012), it is understandable that the low-width slope of the red galaxy WF would be flat or even turn over, because only the most massive red elliptical galaxies will contain enough H I to be detected, therefore boosting the high-width end.

3.3 Error Analysis

We account for a number of sources of error which we add in quadrature; the first is from Poisson counting errors. We also take into account the error in each bin of our bivariate distribution introduced from the 2DSWML method which we estimate via the inverse of the information matrix as described in Efstathiou, Ellis & Peterson (1988). This method

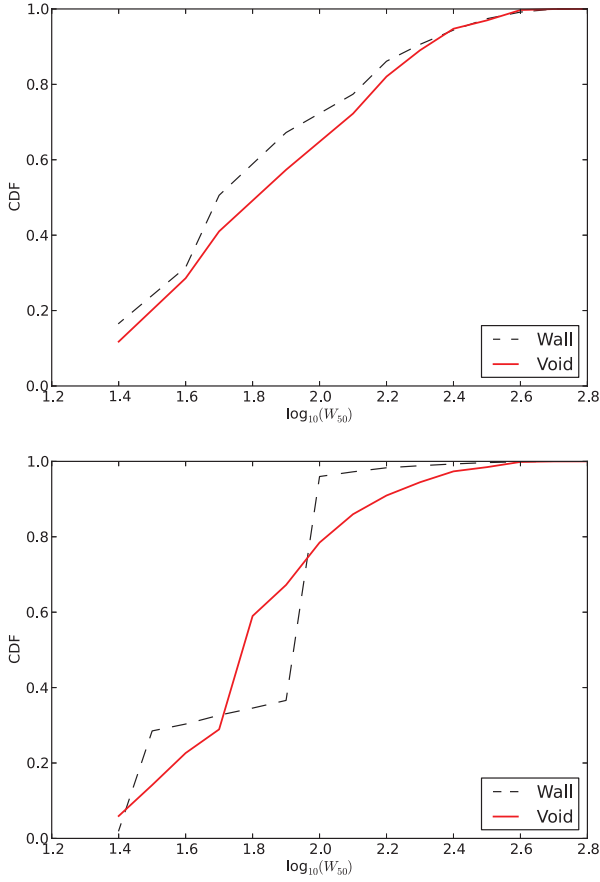


Figure 10. Cumulative distribution function of wall (black dashed) and void (red solid) WF. Top: Outlying points from the distributions have been removed. Bottom: Outlying distribution points are left in the CDF calculation.

uses the fact that the maximum likelihood estimates of ϕ_{jk} are asymptotically normally distributed.

We also account for cosmic variance, or the effects of the inhomogeneity of large scale structure, by using the jackknife resampling method (Efron 1982) to estimate the uncertainties in our HIMF/WF measurements. We do so by dividing the Spring Sky into N subregions, and calculating the HIMF/WF of a subsample of galaxies which omits a different $1/N$ th of the surveyed area each time. After measuring the HIMF/WF of each of the N regions, we estimate the variance of the value of the distribution function in each H I mass/width bin as

$$\text{Var}(x) = \frac{N-1}{N} \sum_{i=1}^N (x_i - \bar{x})^2. \quad (5)$$

For our analysis, we divide our sample volume into $N = 18$ subregions, equally spaced in R.A.

For the HIMF, we need to account for errors in distance measurements. The calculation of the H I mass of a galaxy

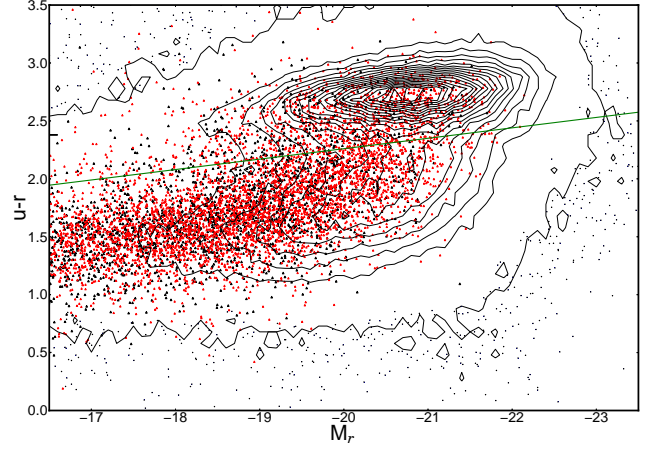


Figure 11. Colour-magnitude diagram of optically-selected and HI-selected galaxies. Contours and black outlying points represent density of SDSS DR7 galaxies. Black and red triangles represent ALFALFA wall and void galaxies respectively. Green line shows the colour cut mentioned in the text that splits the samples into a “red sequence” and a “blue cloud”. The ALFALFA sample is lacking in the red sequence where we find our optical sample to be most dense.

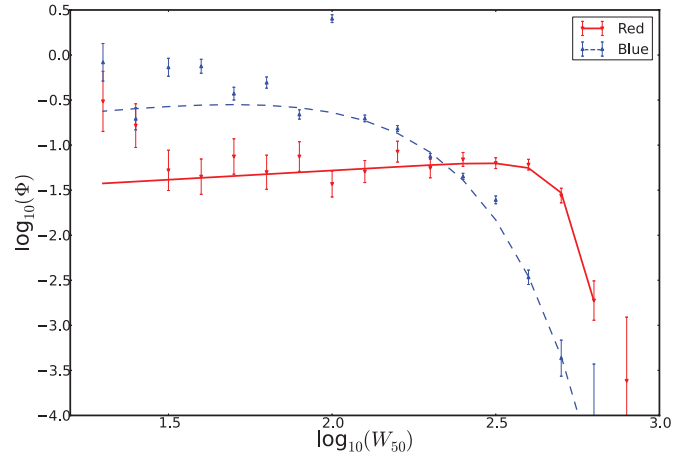


Figure 12. The WF of red (red triangles) and blue (blue triangles) galaxies. The best-fitting modified Schechter functions for each sample are shown as solid (red) and dashed (blue) lines. We see that the low-width slope of the red galaxy WF is substantially flatter than that of the blue sample.

is proportional to the square of the distance to the galaxy; thus, errors in distance estimates could lead to large errors in mass and cause a galaxy to be moved from one mass bin to another. We account for this by creating 300 realizations of the void and wall HIMFs, where we estimate errors on M_{HI} using reported S_{int} errors and estimated distance errors. We give each galaxy i in our sample, at a distance D_i , a random H I mass assuming a Gaussian random error, and calculate the HIMF of each of these realizations.

We use a similar approach to account for the error in velocity widths which can shift a galaxy from one width bin to another, by creating 150 realizations of the void and

wall WFs using the reported W_{50} and ΔW_{50} values. The published W_{50} errors, ΔW_{50} , from the $\alpha.40$ catalog take into account distortion of the spectral profile due to noise and the systematic effect of a guess at the locations of the spectral boundaries.

4 COMPARISON WITH PREVIOUS OBSERVATIONS

4.1 Comparing the HIMF

Previous studies on the environmental impact of the HIMF come to varying conclusions depending on the H I sample used or the method of determining galaxy density. Springob, Haynes & Giovanelli (2005) compare the HIMF of a complete optically-selected sample across environments. The sample consists of H I-selected galaxies with integrated H I flux $S_{int} > 0.6$ within $-2^\circ < \text{Dec} < 38^\circ$ with an optical apparent diameter $a > 1.0'$, Galactic latitude $|b| > 15^\circ$, and morphological type Sa-Irr. The authors define environment based on ranges of galaxy densities (local density: $n < 1.5, 1.5 < n < 3.0, n > 3.0$) defined via a Point Source Catalog Redshift Survey (PSCz) density reconstruction map, and find, with low-significance, that α flattens with increasing density while M^* shifts to lower masses (within a range of $\log(M^*) < 0.16$). This trend is consistent with the theory that galaxies in clusters are H I deficient (Giovanelli & Haynes 1985b), however the decrease in M^* with increasing density contradicts our findings. While these findings are of low statistical significance, and the authors report that better statistics are needed to conclusively determine whether the HIMF varies across environments, differences between our results and theirs could be due to the difference in samples – optically-selected vs. H I-selected samples. The authors also do not isolate “void” galaxies as we have defined them.

Zwaan et al. (2005) compute the HIMF in several density regions using n -th nearest neighbor distances to define density for $n = 1, 3, 5, 10$. They find that the best-fitting Schechter function for low-density environments has a flat low-mass end slope α that steepens with increasing density when defined on small and large scales. They find no environmental dependence of the characteristic turnover mass M^* . This is counterintuitive given that we would expect galaxies in extremely overdense areas to have their gas stripped away during mergers or other galactic interactions. One possible reason for Zwaan et al. (2005) finding such a contrasting result is that the authors define local density using the H I galaxies themselves via nearest neighbor distances. Galaxies living in extremely high-density environments defined by an optical sample may undergo mergers or other astrophysical effects causing most, if not all, H I to be stripped from low mass galaxies, resulting in a very different density map from those found using optical surveys.

Martin (2011) uses both the full $\alpha.40$ dataset as well as the Spring Sky portion of the data to estimate the HIMF of galaxies living in several different density regions. She uses two methods to determine local density: first by using two PSCz density reconstruction maps (a coarse and fine grid), and second by applying an n -th nearest neighbors method to a volume-limited sample of galaxies from SDSS

DR7 over a range of n values, and thus, over a range of density scales. The latter of these methods was only applied to the Spring Sky portion of the dataset where the $\alpha.40$ and SDSS DR7 footprints overlap. Using these methods, Martin (2011) finds that M^* increases with increasing density on all scales, whereas the trend of the low-mass-end slope varies depending on the scale on which environment is defined. When density is defined on larger scales, α steepens with density until some threshold density, after which it flattens out. The author suggests that when density is defined on the largest scales, the HIMF will have a flattened low-mass slope, in the extreme high and low density regions, whereas the not-so-extreme environments will have a relatively steeper slope that increases with density. Martin (2011) proposes the lowest density regions maintain an abundance of intermediate-mass galaxies – possibly due to an increased sensitivity to reionization in voids (Hoeft et al. 2006) – which boosts the intermediate regions of the HIMF thus flattening the slope. In the highest density regions, the lowest mass galaxies have their cool gas stripped away, thus flattening the low-mass slope.

Pisano et al. (2011) use the HICAT (Meyer et al. 2004) catalog and the Lyons Group Galaxies to determine the HIMF of six loose groups of galaxies with properties similar to those of the Local Group. These authors find a very flat low mass slope for loose galactic groups. Stierwalt et al. (2009) use the ALFALFA survey calculate the HIMF of the Leo I Group which has a higher density than the groups used in Pisano et al. 2011. They find a steep low-mass slope of $\alpha = -1.41$. (Kovac 2007) on the other hand, find a very flat low-mass slope of the high-density CV group. There does not seem to be a clear trend with environment at least on the group level.

In the Spring Sky, we investigate the HIMF parameters of true voids – extreme underdensities on the largest scales – and find the characteristic turnover mass M^* is shifted towards lower masses compared to M^* in denser environments. In conjunction with the findings of Stierwalt et al. (2009), who find a relatively steep ($\alpha = -1.41$) low-mass-end of the HIMF for objects in the Leo I group, our findings of the low-mass slope of void galaxies ($\alpha = -1.29$) indicate that the low-mass slope of the HIMF of ALFALFA detections steepens with density. This result is in agreement with the findings of Martin (2011). A number of things could be responsible for the somewhat flatter low-mass slope of void galaxies than wall galaxies. The higher specific star formation rates of low mass galaxies in voids may cause them to burn their fuel faster than their counterparts in walls, thereby flattening the low-mass slope. Given the shift in characteristic H I mass to lower masses in voids, and assuming (again, naively) that the baryonic mass is directly proportional to the DMH mass, void galaxies will have shallower potential wells and could much more easily lose their cool gas, causing their low-mass slope to flatten. Another, more likely, candidate for the cause of the flattened low-mass slope is supernova feedback. While a comparison of optical and infrared redshift surveys (Fisher et al. 1995; Saunders et al. 2000; Strauss et al. 2002; Jones et al. 2004) might reveal similar large-scale structure (Hoyle & Vogeley 2004), local density maps revealing large-scale structure in H I would differ drastically (e.g. Papastergis et al. (2013); Waugh et al. (2002)). Therefore, we cannot quantitatively compare our re-

sults to Zwaan et al. (2005), because they measure local density using an H I sample. We also cannot quantitatively compare our results to those of Springob, Haynes & Giovanelli (2005), because they determine the HIMF using an optically-selected sample.

4.2 Comparing the WF

Little work has been done to determine the environmental effects on purely observed velocity width functions, specifically in the most underdense regimes. Desai et al. (2004) compare the Galaxy Circular Velocity Function (GCVF) of clusters grown in a Λ CDM simulation with the GCVF of clusters from the SDSS obtained using galaxy photometry and the Tully-Fisher relation (Tully & Fisher 1977). They find that both the observed and simulated GCVFs are well fit by a power law, with the observed cluster GCVF having only a slightly shallower slope, although they mention the difference in slope is not significant. They also determine the GCVF of “field” galaxies and find that, compared to the predicted power law, these galaxies display a much shallower slope at low velocities and a much steeper slope at higher velocities with a turnover velocity of $\sim 200 \text{ km s}^{-1}$ – a shape well described by a Schechter function.

Abramson et al. (2013) report their findings on the circular velocity function (CVF) of galaxies in groups using three different samples from the NYU Value Added Galaxy Catalog (Blanton et al. 2005c). In contrast to Λ CDM predictions, these authors find that the group galaxy CVF is consistent with, if not shallower than, the observed field galaxy CVF at the low-velocity end. They find that the shape of the CVF depends primarily on the morphological types of galaxies included in the samples, with an increase in the fraction of late-type galaxies steepening the low-velocity slope; they suggest the flattened slope of the group CVF is due primarily to the depression of late-type galaxies in groups. Sigad et al. (2000) find similar results using a Λ CDM simulation. Assuming a linear relation between halo mass and luminosity, the authors populate the haloes with “galaxies”, identify group and isolated “galaxies”, and report that the isolated “galaxies” have a steeper low-velocity slope than grouped galaxies.

Although we cannot directly compare an observed WF with a CVF, at first glance, our findings on the environmental dependence of the WF appear to be in contrast with Abramson et al. (2013) and Sigad et al. (2000), and indicate that galaxies in voids exhibit a shallower low-velocity slope than their counterparts in denser regions; however, large uncertainties weaken our conclusions. On the other hand, assuming colour and morphology go hand-in-hand, our results are in agreement with those of Abramson et al. (2013) in that blue galaxies seem to have a steep low-velocity width slope and red galaxies tend to have a much shallower low-velocity width slope. See Figure 12 for a comparison of the blue and red WFs.

5 CONCLUSIONS

Using the void catalog obtained by Pan et al. (2012) and the $\alpha.40$ catalog from Haynes et al. (2011), we measure the HIMF of 2,300 void galaxies with H I masses ranging from

$7.2 < \log(M_{\text{HI}}/M_{\odot}) < 10.8$. We find that the HIMF of void galaxies is well fit by a Schechter function with parameters $\Phi^* = (1.37 \pm 0.1) \times 10^{-2} h_{70}^3 \text{ Mpc}^{-3}$, $M_{\text{HI}}^* + 2 \log h_{70} = 9.86 \pm 0.02$, and $\alpha = -1.29 \pm 0.02$. For galaxies residing in higher density regions, we find the best-fitting Schechter parameters to be $\Phi^* = (1.82 \pm 0.03) \times 10^{-2} h_{70}^3 \text{ Mpc}^{-3}$, $M_{\text{HI}}^* + 2 \log h_{70} = 10.00 \pm 0.01$, and $\alpha = -1.35 \pm 0.01$. We also measure the WFs across environments and, while the void and wall WFs are not well fit by a modified Schechter function, we estimate the best-fitting parameters of a modified Schechter function to be $\Phi^* = 0.21 \pm 0.1 h^3 \text{ Mpc}^{-3}$, $\log(W^*) = 2.13 \pm 0.3$, $\alpha = 0.52 \pm 0.5$, and $\beta = 1.3 \pm 0.4$ for the void sample, and $\Phi^* = 0.022 \pm 0.009 h^3 \text{ Mpc}^{-3}$, $\log(W^*) = 2.62 \pm 0.5$, $\alpha = -0.64 \pm 0.2$, and $\beta = 3.58 \pm 1.5$ for the wall sample.

We conclude the following:

1. The ALFALFA $\alpha.40$ catalog yields a higher fraction of void galaxies (33%) than the optically-selected (26%) SDSS DR7 magnitude-limited sample over the same volume. Because these surveys are magnitude limited, the fraction of void galaxies varies with redshift. We know blind-H I surveys preferentially detect blue, late-type galaxies and void regions are also predominantly filled with these blue, spiral galaxies. The red luminous galaxies, typical in the wall sample of an optical survey, are lost when we use an H I-selected sample. This reduction of red galaxies caused by moving from an optically-selected sample to an H I-selected sample, therefore, decreases the raw count of the wall sample, and increases the void fraction for H I-selected samples.

2. Our findings suggest that the characteristic turnover mass of the HIMF is marginally dependent on environment. The characteristic H I mass, M^* , shifts to lower masses in voids by a factor of 1.4; while this shift is small, it is significant. The shift is consistent with extended Press-Schechter theory which states that the mass function should shift to lower masses in underdense regions.

3. We see only a slight difference in the low-mass slopes of void and wall galaxy HIMFs. We believe something may be gleaned from combining our void results with other’s results investigating large-scale, non-void environments. When we couple our void galaxy HIMF with other H I-selected samples from optically-selected environments, such as Stierwalt et al.’s (2009) HIMF of the Leo I group, and Rosenberg & Schneider’s HIMF of galaxies in the Virgo Cluster, we find that the low-mass end slope α varies with environment on the largest scales. This indicates a possible trend with environment (as mentioned in Martin 2011) where the low-mass slope is flat in voids, and increases with density up to some turnover density, where the galaxies within clusters become H I deficient through e.g. galaxy-galaxy interactions.

Our wall HIMF is neither as steep as that found in Stierwalt et al. (2009) nor as flat as the extremely overdense (cluster) HIMFs suggested by Rosenberg & Schneider (2002) and Martin (2011), because we are effectively averaging over all non-void densities. Our wall regions cover a combination of high-density groups made up of early-type galaxies, low-density groups made up of late-type galaxies, and clusters which tend to be H I deficient, just to name a few. This conglomeration of vastly different environments yields a wall HIMF with a low-mass slope somewhere inbetween the flattest and steepest group/cluster slopes reported in the

Author	Sample	Density Measured	Φ^* $\times 10^{-2} h^3 \text{Mpc}^{-3}$	$M_r^* + 2\log h$	α
Rosenberg	ADBS	Full Sample Virgo Cluster	0.58	9.88	-1.53 -1.2
Springob	optically-selected galaxies	PSCz DM: -lowest ρ -intermediate ρ -highest ρ	0.32	10.07 9.91 9.96	\sim -1.37 \sim -1.13 \sim -1.25
Zwaan	HIPASS	H I 10^{th} NN: -lowest ρ -intermediate ρ -highest ρ	0.60	9.80	-1.0 -1.4 -1.55
Martin	ALFALFA	SDSS 10^{th} NN -lowest ρ -intermediate ρ -highest ρ	0.31	9.80 10.05 10.05	-1.15 -1.37 -1.2
Martin	ALFALFA	Coarse PSCz DM: -lowest ρ -higher ρ		9.93 10.05	-1.0 -1.45
Stierwalt	ALFALFA	Leo I Group Full Sample	\sim 3.0	\sim 10.7	-1.41
Pisano	HICAT	Optically-Selected Loose Groups		\sim 9.8	-1.0
this paper	ALFALFA	VoidFinder - Void VoidFinder - Wall	1.37 ± 0.08 0.28 ± 0.03	9.86 ± 0.02 10.00 ± 0.03	-1.29 ± 0.02 -1.35 ± 0.03

Table 1. Schechter function fits to the HIMFs of different galaxy samples across environments. Each sample contains either H I-selected or optically-selected galaxies, and galaxy environment was determined using either Nearest Neighbor algorithms (using optical or H I samples), PSCz density maps, well-known groups/clusters, or VoidFinder.

literature (Pisano et al. 2011; Martin 2011; Stierwalt et al. 2009; Zwaan et al. 2005; Rosenberg & Schneider 2002).

4. We do not find a statistically significant difference in the WF distribution of wall and void galaxies. These distributions are not well fit by a modified Schechter function.

5. We find that the WF varies with galaxy colour with bluer galaxies increasing the low velocity slope. The WF of the blue and red galaxies are also not well fit by a modified Schechter function.

ACKNOWLEDGEMENTS

The authors would like to acknowledge the work of the entire ALFALFA collaboration team in observing, flagging, and extracting the catalog of galaxies used in this work. We thank the referee for helpful comments and suggestions. The ALFALFA team at Cornell is supported by NSF grants AST-0607007 and AST-1107390 to RG and MPH and by grants from the Brinson Foundation.

Funding for the creation and distribution of the SDSS Archive has been provided by the Alfred P. Sloan Foundation, the Participating Institutions, the National Aeronautics and Space Administration, the National Science Foundation, the U.S. Department of Energy, the Japanese Monbukagakusho, and the Max Planck Society. The SDSS Web site is <http://www.sdss.org/>.

The SDSS is managed by the Astrophysical Research Consortium (ARC) for the Participating Institutions. The Participating Institutions are The University of Chicago, Fermilab, the Institute for Advanced Study, the Japan Participation Group, The Johns Hopkins University, the Korean Scientist Group, Los Alamos National Laboratory, the Max-

Planck-Institute for Astronomy (MPIA), the Max-Planck-Institute for Astrophysics (MPA), New Mexico State University, University of Pittsburgh, Princeton University, the United States Naval Observatory, and the University of Washington.

REFERENCES

- Abazajian K. N. et al., 2009, *ApJS*, 182, 543
Abramson L. E., Williams R. J., Benson A. J., Kollmeier J. A., Mulchaey J. S., 2013, *ArXiv e-prints*
Aikio J., Maehoenen P., 1998, *ApJ*, 497, 534
Aragon-Calvo M. A., Szalay A. S., 2013, *MNRAS*, 428, 3409
Aragon-Calvo M. A., van de Weygaert R., Araya-Melo P. A., Platen E., Szalay A. S., 2010, *MNRAS*, 404, L89
Basilakos S., Plionis M., Kovač K., Voglis N., 2007, *MNRAS*, 378, 301
Benson A. J., Hoyle F., Torres F., Vogeley M. S., 2003, *MNRAS*, 340, 160
Blanton M. R., Eisenstein D., Hogg D. W., Schlegel D. J., Brinkmann J., 2005a, *ApJ*, 629, 143
Blanton M. R. et al., 2003a, *ApJ*, 592, 819
Blanton M. R., Lin H., Lupton R. H., Maley F. M., Young N., Zehavi I., Loveday J., 2003b, *AJ*, 125, 2276
Blanton M. R., Lupton R. H., Schlegel D. J., Strauss M. A., Brinkmann J., Fukugita M., Loveday J., 2005b, *ApJ*, 631, 208
Blanton M. R., Roweis S., 2007, *AJ*, 133, 734
Blanton M. R. et al., 2005c, *AJ*, 129, 2562
Cen R., 2011, *ApJ*, 741, 99

- Choi Y.-Y., Han D.-H., Kim S. S., 2010, *Journal of Korean Astronomical Society*, 43, 191
- Colberg J. M. et al., 2008, *MNRAS*, 387, 933
- Conroy C. et al., 2005, *The Astrophysical Journal*, 635, 990
- Croton D. J., Farrar G. R., 2008, *MNRAS*, 386, 2285
- Croton D. J. et al., 2005, *MNRAS*, 356, 1155
- Desai V., Dalcanton J. J., Reed D., Mayer L., Quinn T., Governato F., 2004, *MNRAS*, 351, 265
- Efron B., 1982, *The Jackknife, the Bootstrap, and Other Resampling Plans*. Society for Industrial and Applied Mathematics, Philadelphia, PA
- Efstathiou G., Ellis R. S., Peterson B. A., 1988, *MNRAS*, 232, 431
- El-Ad H., Piran T., 1997, *ApJ*, 491, 421
- El-Ad H., Piran T., 2000, *MNRAS*, 313, 553
- El-Ad H., Piran T., da Costa L. N., 1997, *MNRAS*, 287, 790
- Elyiv A. A., Karachentsev I. D., Karachentseva V. E., Melnyk O. V., Makarov D. I., 2013, *Astrophysical Bulletin*, 68, 1
- Fisher K. B., Huchra J. P., Strauss M. A., Davis M., Yahil A., Schlegel D., 1995, *ApJS*, 100, 69
- Fukugita M., Ichikawa T., Gunn J. E., Doi M., Shimasaku K., Schneider D. P., 1996, *AJ*, 111, 1748
- Geha M., Blanton M. R., Yan R., Tinker J. L., 2012, *ApJ*, 757, 85
- Giovanelli R. et al., 2013, *AJ*, 146, 15
- Giovanelli R. et al., 2005a, *AJ*, 130, 2613
- Giovanelli R. et al., 2005b, *AJ*, 130, 2598
- Giovanelli R. et al., 2007, *AJ*, 133, 2569
- Goldberg D. M., Jones T. D., Hoyle F., Rojas R. R., Vogeley M. S., Blanton M. R., 2005, *ApJ*, 621, 643
- Gottlöber S., Lokas E. L., Klypin A., Hoffman Y., 2003, *MNRAS*, 344, 715
- Grogin N. A., Geller M. J., 1999, *AJ*, 118, 2561
- Gunn J. E. et al., 1998, *AJ*, 116, 3040
- Haynes M. P., 2008, in *Astronomical Society of the Pacific Conference Series*, Vol. 395, *Frontiers of Astrophysics: A Celebration of NRAO's 50th Anniversary*, Bridle A. H., Condon J. J., Hunt G. C., eds., p. 125
- Haynes M. P., Giovanelli R., Chincarini G. L., 1984, *ARA&A*, 22, 445
- Haynes M. P. et al., 2011, *AJ*, 142, 170
- Hoeft M., Yepes G., Gottlöber S., Springel V., 2006, *MNRAS*, 371, 401
- Hoyle F., Rojas R. R., Vogeley M. S., Brinkmann J., 2005, *ApJ*, 620, 618
- Hoyle F., Vogeley M. S., 2002, *ApJ*, 566, 641
- Hoyle F., Vogeley M. S., 2004, *ApJ*, 607, 751
- Hoyle F., Vogeley M. S., Pan D., 2012, *MNRAS*, 426, 3041
- Huang S., Haynes M. P., Giovanelli R., Brinchmann J., 2012, *ApJ*, 756, 113
- Jones D. H. et al., 2004, *MNRAS*, 355, 747
- Karachentsev I. D., Karachentseva V. E., Huchtmeier W. K., Makarov D. I., 2004, *AJ*, 127, 2031
- Karachentseva V. E., Mitronova S. N., Melnyk O. V., Karachentsev I. D., 2010, *Astrophysical Bulletin*, 65, 1
- Kauffmann G., Fairall A. P., 1991, *MNRAS*, 248, 313
- Kent B. R. et al., 2008, *AJ*, 136, 713
- Klypin A., Kravtsov A. V., Valenzuela O., Prada F., 1999, *ApJ*, 522, 82
- Koposov S. E., Yoo J., Rix H.-W., Weinberg D. H., Macciò A. V., Escudé J. M., 2009, *ApJ*, 696, 2179
- Kovac K., 2007, PhD thesis, University of Groningen
- Kreckel K., Joung M. R., Cen R., 2011, *ApJ*, 735, 132
- Loveday J., 2000, *MNRAS*, 312, 557
- Lupton R., Gunn J. E., Ivezić Z., Knapp G. R., Kent S., 2001, in *Astronomical Society of the Pacific Conference Series*, Vol. 238, *Astronomical Data Analysis Software and Systems X*, Harnden Jr. F. R., Primi F. A., Payne H. E., eds., p. 269
- Martin A. M., 2011, PhD thesis, Cornell University, New York, USA
- Martin A. M., Giovanelli R., Haynes M. P., Saintonge A., Hoffman G. L., Kent B. R., Stierwalt S., 2009, *ApJS*, 183, 214
- Martin A. M., Papastergis E., Giovanelli R., Haynes M. P., Springob C. M., Stierwalt S., 2010, *ApJ*, 723, 1359
- Masters K. L., Haynes M. P., Giovanelli R., 2004, *ApJ*, 607, L115
- Mathis H., White S. D. M., 2002, *MNRAS*, 337, 1193
- Melnyk O. V., Karachentseva V. E., Karachentsev I. D., Makarov D. I., Chilingarian I. V., 2009, *Astrophysics*, 52, 184
- Meyer M. J. et al., 2004, *MNRAS*, 350, 1195
- Neyrinck M. C., 2008, *MNRAS*, 386, 2101
- Pan D. C., Vogeley M. S., Hoyle F., Choi Y.-Y., Park C., 2012, *MNRAS*, 421, 926
- Papastergis E., Giovanelli R., Haynes M. P., Rodríguez-Puebla A., Jones M. G., 2013, *ArXiv e-prints*
- Papastergis E., Martin A. M., Giovanelli R., Haynes M. P., 2011, *ApJ*, 739, 38
- Park C., Choi Y.-Y., Kim J., Gott, III J. R., Kim S. S., Kim K.-S., 2012, *ApJ*, 759, L7
- Park C., Choi Y.-Y., Vogeley M. S., Gott, III J. R., Blanton M. R., SDSS Collaboration, 2007, *ApJ*, 658, 898
- Patiri S. G., Prada F., Holtzman J., Klypin A., Betancort-Rijo J., 2006, *MNRAS*, 372, 1710
- Peebles P. J. E., 2001, *ApJ*, 557, 495
- Pisano D. J., Barnes D. G., Staveley-Smith L., Gibson B. K., Kilborn V. A., Freeman K. C., 2011, *ApJS*, 197, 28
- Plionis M., Basilakos S., 2002, *MNRAS*, 330, 399
- Press W. H., Schechter P., 1974, *ApJ*, 187, 425
- Rojas R. R., Vogeley M. S., Hoyle F., Brinkmann J., 2004, *ApJ*, 617, 50
- Rojas R. R., Vogeley M. S., Hoyle F., Brinkmann J., 2005, *ApJ*, 624, 571
- Rosenberg J. L., Schneider S. E., 2000, *VizieR Online Data Catalog*, 213, 177
- Rosenberg J. L., Schneider S. E., 2002, *ApJ*, 567, 247
- Saintonge A., Giovanelli R., Haynes M. P., Hoffman G. L., Kent B. R., Martin A. M., Stierwalt S., Brosch N., 2008, *AJ*, 135, 588
- Saunders W. et al., 2000, *MNRAS*, 317, 55
- Schaap W. E., van de Weygaert R., 2000, *A&A*, 363, L29
- Schechter P., 1976, *ApJ*, 203, 297
- Sheth R. K. et al., 2003, *ApJ*, 594, 225
- Sheth R. K., van de Weygaert R., 2004, *MNRAS*, 350, 517
- Sigad Y., Kolatt T. S., Bullock J. S., Kravtsov A. V., Klypin A. A., Primack J. R., Dekel A., 2000, *ArXiv Astrophysics e-prints*
- Springob C. M., Haynes M. P., Giovanelli R., 2005, *ApJ*, 621, 215
- Stierwalt S., Haynes M. P., Giovanelli R., Kent B. R., Mar-

- tin A. M., Saintonge A., Karachentsev I. D., Karachentseva V. E., 2009, *AJ*, 138, 338
- Strauss M. A. et al., 2002, *AJ*, 124, 1810
- Sutter P. M., Lavaux G., Wandelt B. D., Weinberg D. H., 2012, *ApJ*, 761, 44
- Tinker J. L., Conroy C., Norberg P., Patiri S. G., Weinberg D. H., Warren M. S., 2008, *ApJ*, 686, 53
- Toribio M. C., Solanes J. M., 2009, *AJ*, 138, 1957
- Toribio M. C., Solanes J. M., Giovanelli R., Haynes M. P., Martin A. M., 2011, *ApJ*, 732, 93
- van de Weygaert R., Platen E., Tigrak E., Hidding J., van der Hulst J. M., Aragón-Calvo M. A., Stanonik K., van Gorkom J. H., 2010, in *Astronomical Society of the Pacific Conference Series*, Vol. 421, *Galaxies in Isolation: Exploring Nature Versus Nurture*, Verdes-Montenegro L., Del Olmo A., Sulentic J., eds., p. 99
- Verheijen M. A. W., Trentham N., Tully B., Zwaan M., 2001, in *Astronomical Society of the Pacific Conference Series*, Vol. 240, *Gas and Galaxy Evolution*, Hibbard J. E., Rupen M., van Gorkom J. H., eds., p. 507
- von Benda-Beckmann A. M., Müller V., 2008, *MNRAS*, 384, 1189
- Warren M. S., Abazajian K., Holz D. E., Teodoro L., 2006, *ApJ*, 646, 881
- Waugh M. et al., 2002, *MNRAS*, 337, 641
- Zavala J., Jing Y. P., Faltenbacher A., Yepes G., Hoffman Y., Gottlöber S., Catinella B., 2009, *ApJ*, 700, 1779
- Zwaan M. A., Meyer M. J., Staveley-Smith L., 2010, *MNRAS*, 403, 1969
- Zwaan M. A., Meyer M. J., Staveley-Smith L., Webster R. L., 2005, *MNRAS*, 359, L30